AGU PUBLICATIONS

Geophysical Research Letters

RESEARCH LETTER

10.1002/2014GL060136

Key Points:

- First one-step vertical NO_2 column retrieval from a new direct fitting algorithm
- A new spatial technique for reliable stratosphere-troposphere NO_2 separation
- Demonstration of sensitive global tropospheric NO_2 measurements from SNPP OMPS

Correspondence to:
K. Yang,
KaiYang@umd.edu

Citation:
Yang, K., S. A. Carn, C. Ge, J. Wang, and R. R. Dickerson (2014), Advancing measurements of tropospheric NO_2 from space: New algorithm and first global results from OMPS, *Geophys. Res. Lett.*, *41*, 4777–4786, doi:10.1002/2014GL060136.

Received 4 APR 2014
Accepted 15 JUN 2014
Accepted article online 18 JUN 2014
Published online 10 JUL 2014

Advancing measurements of tropospheric NO_2 from space: New algorithm and first global results from OMPS

Kai Yang[1], Simon A. Carn[2], Cui Ge[3], Jun Wang[3], and Russell R. Dickerson[1]

[1]Department of Atmospheric and Oceanic Science, University of Maryland College Park, College Park, Maryland, USA, [2]Department of Geological and Mining Engineering and Sciences, Michigan Technological University, Houghton, Michigan, USA, [3]Department of Earth and Atmospheric Sciences, University of Nebraska-Lincoln, Lincoln, Nebraska, USA

Abstract We present a new algorithm based on the iterative spectral fitting technique for direct retrieval of nitrogen dioxide (NO_2) vertical columns from hyperspectral satellite measurements, and a new spatial technique for separating the stratospheric and tropospheric contributions to the total NO_2 vertical columns. This direct vertical column fitting (DVCF) algorithm allows more complete treatment of underlying algorithm physics compared to the differential optical absorption spectroscopy technique and enables more accurate accounting for the effects of spectral and altitude variations in NO_2 measurement sensitivities. This DVCF algorithm and the stratosphere-troposphere separation scheme are applied to ultraviolet measurements from the Nadir Mapper of the Ozone Mapping and Profiler Suite (OMPS) on the Suomi National Polar-orbiting Partnership spacecraft. The first results demonstrate the potential of OMPS for sensitive global monitoring of tropospheric NO_2. Comparisons show good agreement with Aura Ozone Monitoring Instrument (OMI) tropospheric NO_2 data and that OMPS data have sufficient quality to continue and extend OMI NO_2 data records.

1. Introduction

Nitrogen dioxide (NO_2) is an important constituent in the stratosphere and troposphere. In the stratosphere, it catalyzes ozone destruction [*Brühl and Crutzen*, 2000], and in the troposphere it is a precursor of tropospheric ozone (produced by its reaction with volatile organic compounds, VOCs) and nitric acid (HNO_3), formed by its reaction with the hydroxyl radical (OH) or heterogeneous reaction with nitrogen pentoxide (N_2O_5) [*Seinfeld and Pandis*, 2006]. The major sources of tropospheric NO_x ($NO+NO_2$) are fossil fuel (coal, oil, and gas) combustion, biomass burning, lightning, and microbial production in soils. NO_2 in the lower troposphere and its chemically transformed products (such as tropospheric O_3 and nitrate aerosols) are air pollutants that are hazardous to human health and are harmful to the environment. Observations of tropospheric NO_2, which has a short atmospheric lifetime (from several hours in summer to tens of hours in winter [*Beirle et al.*, 2003; *Lamsal et al.*, 2010]), provide key information about emission sources of air pollutants and air quality.

Global distribution of tropospheric NO_2 has been measured since the mid-1990s from a number of polar-orbiting satellite instruments, including the Global Ozone Monitoring Experiment (GOME, 1995–2003) [*Burrows et al.*, 1999] on ERS-2, the Scanning Imaging Absorption Spectrometer for Atmospheric Chartography (SCIAMACHY, 2002–2012) [*Bovensmann et al.*, 1999] on ENVISAT, the Ozone Monitoring Instrument (OMI, 2004 to the present) [*Levelt et al.*, 2006] on Aura, and GOME-2 [*Callies et al.*, 2000; *Munro et al.*, 2006] on METOP-A (2006 to the present) and METOP-B (2012 to the present). The long-term data set from these instruments provides a unique reference for monitoring changes in global tropospheric NO_2 distributions [*Richter et al.*, 2005; *Hilboll et al.*, 2013]. It is important to continue and improve satellite measurements of NO_2, by advancing retrieval techniques that are capable of extracting more accurate geophysical information from the spectral measurements of past, present, and future satellite missions. In this paper, we first describe a new NO_2 retrieval algorithm, and a new scheme for separating the stratospheric and tropospheric NO_2 contributions to the retrieved total vertical columns. Next we present results from the application of this algorithm to the measured ultraviolet (UV) spectra from the Nadir Mapper of the Ozone Mapping and Profiler Suite (OMPS) onboard the Suomi National Polar-orbiting Partnership (SNPP) satellite and demonstrate its capabilities for global monitoring of NO_2. Comparisons with NO_2 results retrieved from OMI visible measurements are shown next. We summarize our findings and discuss future work in the last section.

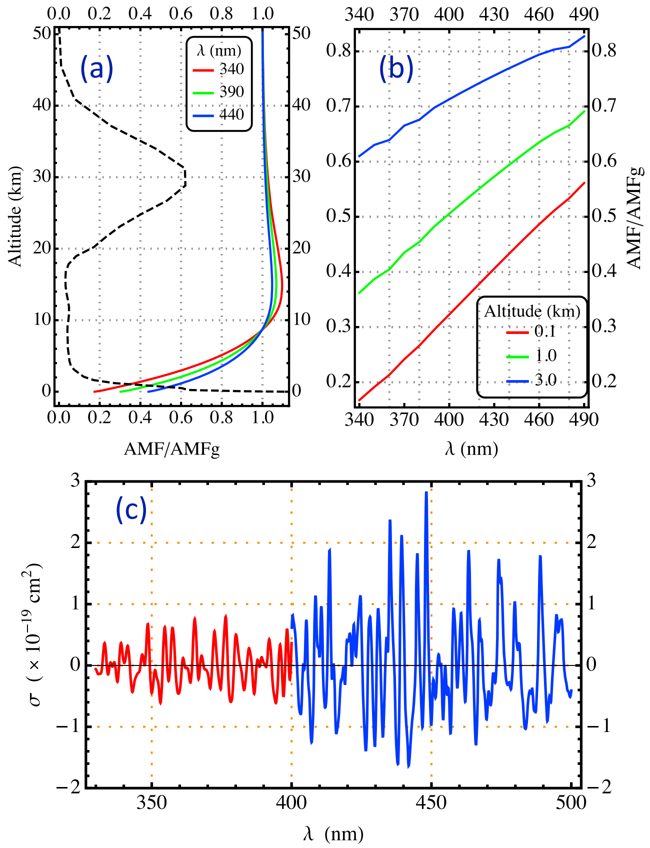

Figure 1. The altitude-resolved AMF, normalized by the geometric air mass factor (AMFg). (a) AMFs for three wavelengths (340, 390, and 440 nm) are plotted for an altitude range between 0 and 50 km. (b) AMFs at three altitudes (0.1, 1.0, and 3.0 km) are plotted as a function of wavelength in the range between 340 and 490 nm. These AMFs are computed using the TOMRAD radiative transfer code [*Dave*, 1965], for a surface albedo of 0.1, a solar zenith angle of 45°, a viewing zenith angle of 20°, and a relative azimuth angle of 45°. A sample NO_2 vertical profile (dotted black curve) from GEOS-Chem monthly mean climatology is plotted in Figure 1a. (c) NO_2 differential cross sections at 220 K are plotted: convolution with OMI slit function (~0.63 nm spectral resolution) is applied above 400 nm (blue curve) and with OMPS NM slit (~1.1 nm spectral resolution) below 400 nm (red curve).

2. The OMPS Nadir Mapper Instrument

OMPS Nadir Mapper (NM), flying on the SNPP spacecraft since October 2011, is a hyperspectral UV spectrometer designed primarily to measure global total ozone, and it will be flown on the next two NOAA and NASA Joint Polar Satellite System satellites: JPSS-1 and JPSS-2, scheduled to launch in 2017 and 2022, respectively. This nadir-viewing hyperspectral instrument measures backscattered UV radiance spectra, covering the 300–380 nm wavelength range with a spectral resolution of 1 nm and a sampling rate of 0.42 nm per pixel. SNPP is in a Sun-synchronous orbit with a local ascending (northbound) equator crossing time at 1:30 P.M., about 10 to 15 min earlier than the Aura satellite carrying the OMI instrument in the same orbital plane but at a lower altitude. As a result, OMPS NM observations at low to middle latitudes are taken in the afternoon (local time), close in time to OMI observations. OMPS NM provides contiguous daily global coverage in about 14 orbits using a two-dimensional charge-coupled device detector array that scans a 2800 km cross-track swath (110° field of view), divided into 35 instantaneous fields of views (IFOVs) or pixels, which have a ground footprint size of 50 km × 50 km at nadir, similar to that of GOME-2 but larger than that of OMI. One orbit of OMPS NM observations contains about 400 cross-track swaths, each scanning ~7.5 s along track, from southern to northern terminator on the sunlit side of the Earth.

Even though its spectral resolution is coarser, and its spectral sampling frequency is lower than those of its predecessors (GOME, SCIAMACHY, OMI, and GOME-2), we have shown that OMPS NM is uniquely suitable for SO_2 measurements and provides high-quality pollution SO_2 data in the planetary boundary layer [*Yang et al.*, 2013], in addition to SO_2 clouds from volcanic eruptions. Building on this success, we further exploit the capabilities of OMPS NM UV measurements for global monitoring of NO_2.

3. Direct Vertical Column Fitting Algorithm

The NO_2 molecule has distinctive temperature-dependent absorption cross sections (σ) in a broad spectral range covering the near infrared, visible, and UV [*Burrows et al.*, 1998; *Vandaele et al.*, 1998; *Bogumil et al.*, 2003]. Remote sensing has exploited its differential absorption signature (see Figure 1c) for NO_2 detection and quantification. Existing retrieval of tropospheric NO_2 vertical columns from nadir-viewing satellite instruments is accomplished following this procedure: first, slant column amounts are estimated from the observational data using the Differential Optical Absorption Spectroscopy (DOAS) fitting technique

[*Platt*, 1994], then slant columns are separated into stratospheric and tropospheric components, and finally, the tropospheric components are converted into vertical columns using tropospheric air mass factors (AMFs) [*Leue et al.*, 2001; *Velders et al.*, 2001; *Richter and Burrows*, 2002; *Martin et al.*, 2002; *Beirle et al.*, 2003; *Bucsela et al.*, 2006; *Boersma et al.*, 2007; *Richter et al.*, 2011]. This DOAS approach relies on an implicit assumption: the AMFs are independent of wavelength across the fitting window, leading to errors in the retrieved vertical columns when the spectral dependence of AMFs is significant.

In this section, we describe a new approach for NO_2 retrieval, which is adapted from the iterative spectral fitting (ISF) algorithm [*Yang et al.*, 2009a, 2009b, 2010, 2013], initially developed for simultaneous retrieval of ozone (O_3) and sulfur dioxide (SO_2) vertical columns. This direct vertical column fitting (DVCF) approach estimates trace gas vertical columns and other geophysical parameters by adjusting them iteratively until the difference between the satellite-measured Earth view radiance spectra, and those simulated using an accurate radiative transfer model are minimized. This general procedure is not limited to O_3 and SO_2 and can be used for retrieval of other trace gases (including NO_2) when it is applied to the spectral range that is sensitive to their absorptions.

The key improvement of the DVCF approach over the DOAS method lies in the more complete treatment of underlying algorithm physics [*Chance*, 2006]. A measured radiance spectrum consists of photons of different wavelengths that are either backscattered by atmospheric constituents (air molecules, aerosols, or clouds) or reflected by ground or water surfaces. The measurement sensitivity to a NO_2 layer depends on the fraction of the backscattered photons that have passed through this layer on their way to the detectors; therefore, it depends on the layer altitude as the air density varies with atmospheric pressure and temperature and on the wavelength (λ) due to the strong spectral dependence of Rayleigh scattering (with a cross section proportional to $\frac{1}{\lambda^4}$). This measurement sensitivity also depends on the spectral reflectance of the surfaces, the amount and type of clouds and aerosols, and their vertical distributions. The iterative radiative transfer modeling of the measured spectra performed in the DVCF retrieval allows accurate determination of the average photon path lengths (i.e., AMFs) for each wavelength, thus accounting for the effects of spectral and altitude variations in trace gas measurement sensitivity.

Because of the altitude dependence of measurement sensitivity, accurate retrieval of NO_2 vertical columns requires the knowledge of the NO_2 vertical distribution. In the DVCF approach, we use a set of shape factors (S_z) [*Palmer et al.*, 2001; *Martin et al.*, 2004], which are normalized relative vertical distributions, to place constraints on NO_2 vertical distributions. These shape factors are used in the calculation of vertical column weighting functions (WFs), and the retrieval of NO_2 vertical columns (V) can be accomplished with the least squares solution to the set of linear equations composed of measurements for all wavelengths in the fitting window, one of which can be written as

$$\begin{aligned}\ln I_m(\lambda) - \ln I_{\mathrm{TOA}}(\lambda) = V \int_0^\infty \frac{\partial \ln I_{\mathrm{TOA}}(\lambda)}{\partial \tau_z} S_z \sigma(\lambda, T_z) \mathrm{d}z \\ - \sum_i \xi_i \sigma_i(\lambda, T_i) + \epsilon. \end{aligned} \tag{1}$$

Here I_m is the measured reflectance spectrum (i.e., the ratio of radiance to measured irradiance), and I_{TOA} is the modeled reflectance spectrum, without including absorptions of trace gas species, at the top of the atmosphere (TOA); T_z is the atmospheric temperature, a function of altitude (z); and ϵ is the total error, a combination of measurement and model errors. The expressions in equation (1) provide a contrast between DVCF and DOAS retrievals: the first term on the right-hand side (RHS) represents direct vertical column retrieval through fitting of spectrally and vertically weighted cross sections, i.e., the vertical column WF, $\int_0^\infty \frac{\partial \ln I_{\mathrm{TOA}}(\lambda)}{\partial \tau_z} S_z \sigma(\lambda, T_z) \mathrm{d}z$, while the second term accounts for additional trace gas (e.g., O_3, HCHO, BrO, and OClO) absorptions, showing that the slant column, ξ_i of the ith trace gas, is obtained by fitting its molecular absorption cross section σ_i at a specific temperature T_i. The layer optical thickness Jacobian $-\frac{\partial \ln I_{\mathrm{TOA}}(\lambda)}{\partial \tau_z}$, is the altitude-resolved AMF (m_z), and its product with the cross section ($\sigma(\lambda, T_z)$) is the absorber layer measurement sensitivity (K_z). The product of K_z and a layer column (VS_z) specifies the magnitude of trace gas absorption signal from this layer that is carried onto the measured spectra. Examples of m_z are shown in Figure 1, illustrating its significant spectral dependence that varies with altitude in the troposphere, especially in the boundary layer where anthropogenic NO_2 is located. However, m_z is close to the geometric AMF for all wavelengths in the stratosphere, indicating that radiance spectra are insensitive to stratospheric profile shape. In general, DVCF enables a better spectral fit to the measured spectra, because the vertical column WF properly accounts for the magnitude of trace gas absorptions in the measured spectra, enabling a more accurate retrieval of the vertical column, than the DOAS approach for the same species. The central difference between DVCF and DOAS retrievals is the use of spectrally dependent AMFs. To show this, by neglecting the spectral dependence of m_z, the first term on the RHS in (1) can be written as $-V \cdot \mathrm{AMF} \cdot \sigma(\lambda, T_0)$, which is the same expression as the second term on the RHS. Here the AMF for slant column conversion is equal to AMF$= \int_0^\infty m_z S_z \alpha(z) \mathrm{d}z$, where $\alpha(z)$ is the temperature-correction factor, assuming that a factorization can be obtained, such that $\sigma(\lambda, T_z) = \sigma(\lambda, T_0)\alpha(z)$. Note that the DOAS approach yields additional retrieval errors when temperature-dependent absorption cross sections cannot be well approximated with this factorization. It is evident from the general behavior of m_z (see Figures 1a and 1b), the fitting uncertainty resulted from neglecting the spectral dependence of AMF increases in general with fitting window at shorter wavelengths and with larger sizes. Moreover, the standard DOAS method tends to underestimate the absorber (NO_2) vertical column when its loading is very high (e.g., over areas of heavy air pollution), mainly because this method also neglects the column dependence of AMF, which reduces with increasing absorptions. In contrast, these spectral and nonlinear effects are correctly accounted for in the ISF technique, which is capable of using all available spectral measurements for accurate retrieval in the full range absorber concentrations [*Yang et al.*, 2009a].

We use the independent pixel approximation [*Cahalan et al.*, 1994] for partly cloudy observations and calculate the individual components of I_{TOA} for ground and cloud using the TOMRAD radiative transfer model [*Dave*, 1965] with added contributions from rotational Raman scattering (RRS) calculated using the LIDORT-RRS radiative transfer code [*Spurr et al.*, 2008]. To account for the combined effects of surface reflection and atmospheric scattering without explicitly including clouds and/or aerosols in the forward model computation, the DVCF approach derives the albedo and the pressure of the underlying boundary in cloud-free and fully cloud-covered instantaneous fields of view (IFOVs), or the cloud fraction and cloud pressure for the partially cloudy IFOV, including the spectral variation of the albedo or cloud fraction within the spectral range used in the retrieval. These derived quantities, which are consistent with the radiance measurements, facilitate the correct treatment of measurement sensitivity effects. For instance, they are used to estimate the sensitivity reduction due to the partial shielding of trace gases located below the scattering particles, as well as sensitivity enhancement for trace gases located at higher altitudes. Note that *Buchwitz et al.* [2000] developed a similar algorithm, called the weighting function DOAS (WF-DOAS) method, which has been applied to GOME data for total column O_3 retrieval [*Coldewey-Egbers et al.*, 2005] and to SCIAMACHY data for SO_2 retrieval [*Lee et al.*, 2008]. The main difference between these two approaches is in the calculations of WFs: the WF-DOAS uses auxiliary quantities, such as surface albedo and cloud fraction and height, derived usually from different spectral ranges or taken from climatological databases, while the ISF technique retrieves these quantities from the measured spectra to achieve self-consistency between simulations and measurements.

The instrument effect on the retrieval is accounted for in the modeled reflectance spectrum I_{TOA}, and its layer measurement sensitivity K_z through the solar irradiance weighted convolution with the instrument spectral response (slit) function. In the DVCF algorithm, an assisted interpolation technique is used to obtain accurate irradiance values at radiance wavelengths, thereby eliminating the need for undersampling correction [*Chance et al.*, 2005] in the fitting process. This technique relies on a modeled solar spectrum, which is constructed from a solar reference spectrum [e.g., *Chance and Kurucz*, 2010] by the convolution of an instrument slit function. The assisted interpolation is accomplished following this procedure: (1) wavelength calibrations are performed on the measured spectra (both radiance and irradiance) to correct possible wavelength registration errors, (2) the ratios (ρ) of measured to modeled irradiance are computed at the calibrated irradiance wavelengths, and (3) the interpolated irradiance value at a given (calibrated) radiance wavelength is obtained by the product of modeled irradiance and the interpolated ρ. Closure polynomials may also be subtracted from both sides of equation (1) to reduce the effects of calibration and forward model errors, thereby relying on the differential structures of the column WF and the absorption cross sections to quantify the column amounts from the high-frequency structures of the radiance residuals, which are less affected by calibration errors.

The violet blue (410–460 nm) spectral range is commonly used in NO_2 retrieval from satellite measurements, because NO_2 absorption cross sections have large differential structures in this range, as illustrated in Figure 1c, in which high-pass filtered NO_2 cross sections at 220 K [*Vandaele et al.*, 1998] are plotted. Taking the band-pass effects into account, the differential structures between 410 and 460 nm are about 3 times larger than those between 345 and 380 nm. Based on this difference, the stratospheric NO_2 measurement sensitivity (K_z) is about 3 times higher for OMI than that for OMPS. For tropospheric NO_2, K_z is further reduced for both OMI and OMPS because m_z decreases significantly near the surface when its albedo is low (see Figures 1a and 1b). This reduction is larger at shorter wavelengths due to stronger Rayleigh scattering. Thus, OMPS tropospheric K_z is much lower than that of OMI, about 5 to 10 times less sensitive, compounding by the typically lower UV surface albedo. The lower K_z and its steeper altitude gradient in the troposphere imply that OMPS retrieval relies more on the accuracy of the tropospheric shape factor.

4. Stratosphere-Troposphere Separation

The basic premise of Stratosphere-Troposphere Separation (STS) is that the spatial distribution of stratospheric NO_2 is more homogeneous than that of tropospheric NO_2 due to localized emissions and short lifetime of the latter. A number of spatial techniques have been developed to separate the stratospheric and tropospheric contributions to NO_2 slant columns, including the reference sector method [*Richter and Burrows*, 2002; *Martin et al.*, 2002], the wave-2 stratospheric model [*Bucsela et al.*, 2006], the spatial interpolation method [*Bucsela et al.*, 2013] and the cloud-slicing technique [*Choi et al.*, 2014].

In this section, we describe a new spatial technique: an orbit-based approach for STS refinement. An initial STS is performed with the retrieved total vertical columns, which are partitioned into stratospheric (V_s^i) and tropospheric components using tropopause inputs and the a priori shape factors. These initial stratospheric and tropospheric columns usually contain errors due to the mismatch between the actual NO_2 vertical distribution in an IFOV and the a priori shape factor. By analyzing the spatial distribution of the initial stratospheric columns, the shape factor prescription mismatches can be identified and then corrected. Specifically, the high-frequency structures (excluding measurement noise) detected in the retrieved stratospheric NO_2 field are attributed to signals from the troposphere due to imperfections in shape factor prescription, and smoothing them out yields more accurate stratospheric and tropospheric NO_2 vertical columns. To accomplish this, two smooth stratospheric fields are constructed from the initial field for each cross-track position of an orbit of satellite data using the sliding median correction technique [*Yang et al.*, 2007] (first developed for SO_2 retrieval). The values of these two smoothed fields at each pixel are taken to be the median values of two sliding group pixels centered on the selected pixel, covering two latitude bands, about 2 and 20°, respectively, along the orbital track. The spatial extent of the larger latitude band is reduced when the selected pixel is near the terminator to ensure that a roughly equal number of pixels on either side of the selected pixel are included. The smaller latitude band is used to generate a smoothed field (m_h) that retains possible tropospheric signals but without the intrinsic noise in the measurements, while the larger one is used to construct a smoothed field (m_l) with minimal tropospheric contributions, by obtaining the median value from a group of predominantly background pixels, i.e., pixels with little or no elevated tropospheric NO_2. To ensure this condition is satisfied even for large regions (e.g., China and Europe) with elevated tropospheric NO_2, the size of latitude band may be increased (up to 30°), and/or the pixels with elevated NO_2 based on initial retrievals maybe be excluded in the median calculations. Thus, the excesses (+) and deficits (−) of stratospheric NO_2 are obtained from the difference between the two smoothed fields ($m_l - m_h$). The tropospheric columns are then adjusted: stratospheric excesses are added to and deficits are subtracted from the tropospheric fields, while accounting for their different measurement sensitivities. Algebraically, the corrected stratospheric NO_2 column is equal to $V_s = V_s^i + (m_l - m_h)$, and the corresponding tropospheric NO_2 columns (V_t) are retrieved by solving a new set of linear equations:

$$\ln \frac{I_m(\lambda)}{I_{\mathrm{TOA}}(\lambda)} + V_s \int_{z_{\mathrm{tp}}}^{\infty} m_z(\lambda) S_z \sigma(\lambda, T_z) \mathrm{d}z + \sum_i \xi_i \sigma_i(\lambda, T_i) = -V_t \int_0^{z_{\mathrm{tp}}} m_z(\lambda) S_z \sigma(\lambda, T_z) \mathrm{d}z + \epsilon, \tag{2}$$

where z_{tp} is the tropopause altitude.

5. OMPS NM: First Results and Comparisons

We have applied the DVCF algorithm and the STS refinement technique to retrieve stratospheric and tropospheric NO_2 vertical columns from OMPS NM. NO_2 vertical columns, slant columns of other trace gases (O_3, HCHO, BrO, and OClO), and the surface parameters, including the pressure and spectral albedo or cloud fraction of the underlying surfaces are retrieved from the spectral measurements between 345 and 378 nm. Note that a fifth-order polynomial is fitted to filter out low-frequency components from both sides of equation (1) in the retrieval process.

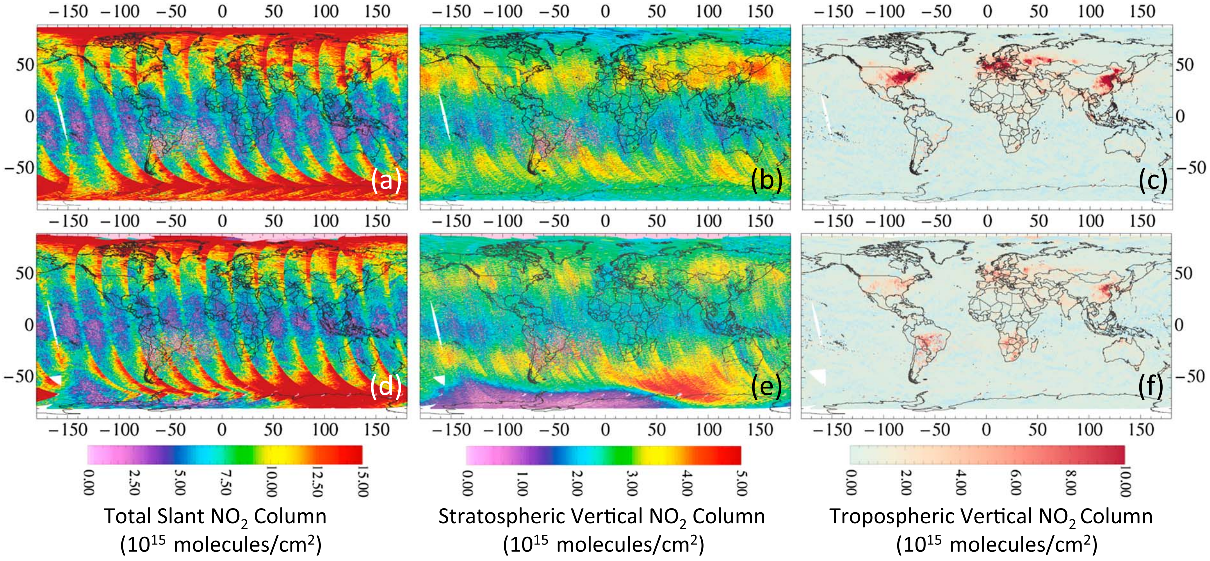

Figure 2. (a, d) Total slant, (b, e) stratospheric vertical, and (c, f) tropospheric vertical NO_2 columns from OMPS NM for 2 days: 21 March 2013 as shown in Figures 2a–2c and 22 September 2013 as shown in Figures 2d–2f.

The a priori NO_2 profile (e.g., see Figure 1a) for an IFOV is selected from a set of monthly mean GEOS-Chem [*Bey et al.*, 2001] shape factors based on time and location. These shape factors are average NO_2 vertical fields within 1300 and 1500 local time from v9-01-01 GEOS-Chem global simulation for 2012 at a coarse resolution (2°latitude × 2.5° longitude).

Sample results are shown in Figure 2, including total NO_2 slant, stratospheric vertical, and tropospheric vertical column densities for 2 days in different seasons, spring (21 March) and fall (22 September), in 2013. Slant, rather than vertical columns are shown here as diagnostics of the spectral content in OMPS observations. Since a slant column provides an estimate of trace gas abundance along the mean photon path from the Sun to the satellite, tropospheric enhancements clearly observed in Figures 2a and 2d over China, Europe, and the United States are direct evidence of OMPS's ability to detect tropospheric NO_2. Figures 2b and 2e are the stratospheric NO_2 distributions, showing that large-scale spatial (both latitudinal and longitudinal) variations of stratospheric NO_2, without the prominent features of local tropospheric enhancements (seen in Figures 2c and 2f, which are removed by the sliding median STS refinement). A polar vortex is observed in Figure 2e, showing an area of low stratospheric NO_2 that is slightly shifted over the Antarctic region, and surrounded by strong stratospheric NO_2 enhancements. This illustrates that the sliding median STS refinement is able to capture large gradients in stratospheric NO_2, providing a reliable representation of its spatial structure. Tropospheric NO_2 columns are displayed in Figures 2c and 2f, showing enhanced values, which are stronger in March than in September over the areas in the Northern Hemisphere with anthropogenic pollution. Tropospheric enhancements from biomass burning are also found over Southern Hemisphere regions in September (Figure 2f). These daily maps demonstrate that OMPS is capable of sensitive global tropospheric NO_2 observations.

To further illustrate the quality of OMPS NO_2 measurements, we show in Figure 3 the gridded monthly mean tropospheric NO_2 vertical columns derived from the OMI standard product (OMNO2 version 2.1 collection 3, available at http://disc.sci.gsfc.nasa.gov/Aura/data-holdings/OMI/omno2_v003.shtml) and from OMPS for 2 months: July and December 2013. Cloud screening is applied to both OMI and OMPS: IFOVs with radiative cloud fraction > 0.3 are excluded. OMI data affected by the row anomaly are also excluded. The value at each grid cell (0.25° × 0.25°, for both OMI and OMPS) is the weighted average of the remaining IFOVs that have overlap with the grid cell. The weight is the observation coverage, defined as the ratio of the cell-IFOV overlap area to the IFOV area. Thus, IFOVs near the swath center are weighted more than those at the edge. These average distributions provide more reliable mapping of persistent tropospheric NO_2 enhancements during these two months. Similar to the daily maps in Figures 2c and 2f, both OMI and OMPS monthly means (Figure 3) show significant enhancements of NO_2 over major industrial and densely populated areas like the United States East Coast, western Europe, East Asia, the Persian Gulf area, northern India and Pakistan, and

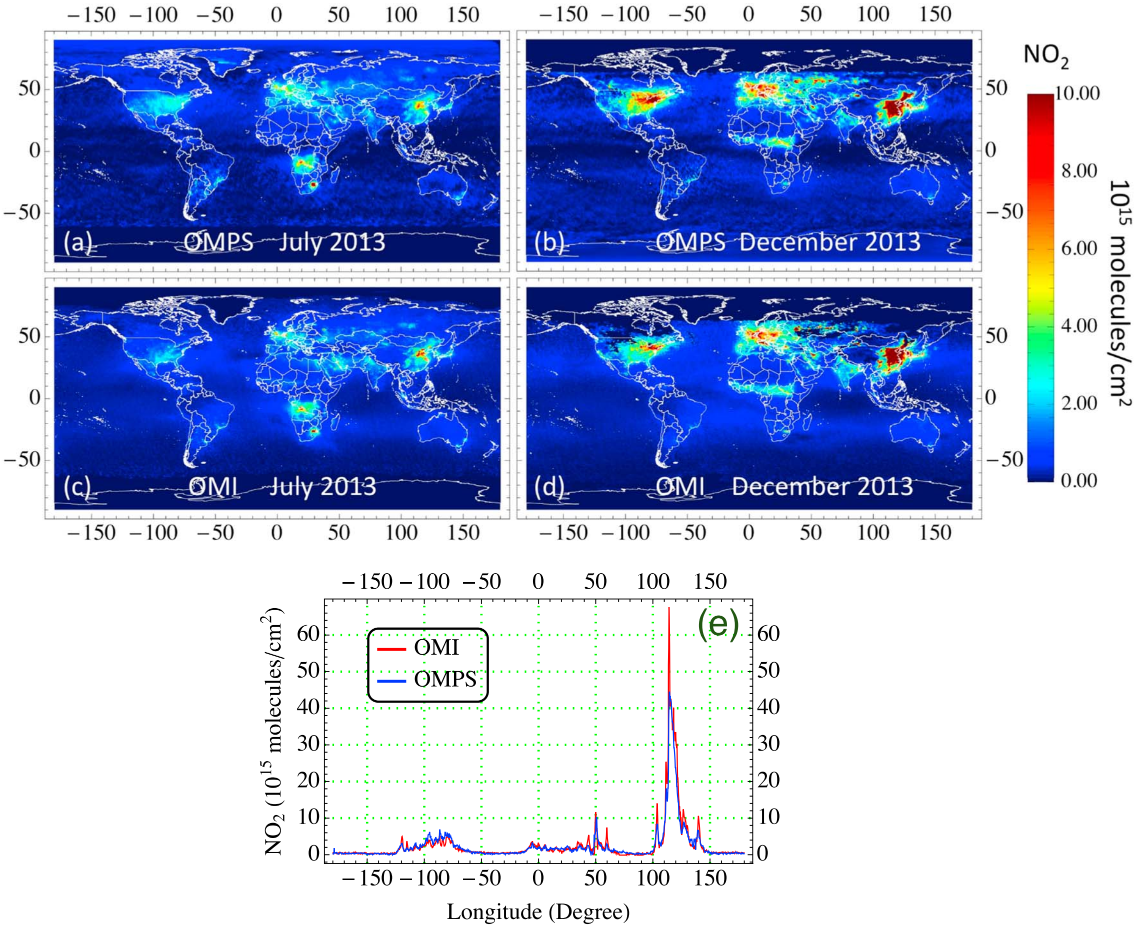

Figure 3. Monthly averages of tropospheric NO_2 vertical columns measured (a, b) by OMPS NM and (c, d) by OMI (NASA standard product) for July and December 2013 over the globe, on a 0.25° × 0.25° latitude-longitude grid. (e) Comparison between OMPS and OMI monthly (December 2013) averages of tropospheric NO_2 vertical columns at 36°N, from 180°W to 180°E.

South Africa. Both OMPS and OMI maps also exhibit tropospheric NO_2 enhancements in some metropolitan areas, such as Melbourne, southern California, and the Seattle/Vancouver region. The seasonal changes are well captured in the monthly means, showing stronger enhancements in the Northern Hemisphere in December than in July, but the opposite in the Southern Hemisphere. Both OMPS and OMI maps also show NO_2 enhancements in central Africa and Brazil in July and in the Sahel region (northern equatorial Africa) in December from biomass burning.

In Figure 3e, we plot the longitudinal variations in the December mean tropospheric NO_2 for both OMI and OMPS, across the map (Figure 3d) at 36°N, where the highest OMI mean value for December is found. While OMI values are higher than those of OMPS over China (between 100° and 150°) at this latitude, these tropospheric NO_2 enhancements agree very well over the U.S. (between −130° and −70°) and Europe (between −10° and 70°). The similarity between OMI and OMPS in spatial distribution over the globe for both months (Figures 3a–3d) and the good quantitative agreement shown in Figure 3e highlight the capabilities of OMPS, which achieves a high tropospheric NO_2 measurement sensitivity that is comparable to that of OMI. The slant column precision is about 0.9×10^{15} mol/cm^2, slightly worse than that (0.75×10^{15} mol/cm^2) for OMI [*Boersma et al.*, 2007], while the precision for the tropospheric vertical columns for OMPS is estimated to be 0.3×10^{15} mol/cm^2, better than that ($\sim 1 \times 10^{15}$ mol/cm^2) for OMI. The similar slant column precisions can be partially explained by the higher OMPS signal-to-noise ratio, ~2500 [*Seftor et al.*, 2014], which is about twice as large as that for OMI [*Levelt et al.*, 2006], compensating for the lower NO_2 measurement sensitivity in OMPS spectral range. However, the lower tropospheric precision for OMI is caused by its STS approach [*Bucsela et al.*, 2013], which produces a smooth (or noise-free) stratospheric field, leaving the intrinsic measurement noise in the tropospheric NO_2 columns.

6. Summary

We have presented a new algorithm and a new STS scheme for improving NO_2 retrieval from satellite-measured UV Earthshine spectra. This DVCF algorithm allows a more complete treatment of underlying algorithm physics compared to the DOAS algorithm and accounts more accurately for the effects of spectral and altitude variations in measurement sensitivities. The STS scheme is shown to be capable of capturing the large-scale structures of the stratospheric NO_2 field and reducing the local features from tropospheric NO_2, thereby improving the tropospheric NO_2 measurements. These general approaches can be applied to spectral (both UV and visible) measurements from past, present, and future satellite missions to improve the long-term global NO_2 data records.

We have applied the DVCF and STS approaches to UV measurements from SNPP/OMPS NM. The first results highlight the potential of OMPS for global monitoring of tropospheric NO_2. Comparisons show good agreement between OMPS and OMI tropospheric NO_2 data and demonstrate that OMPS provides high tropospheric NO_2 measurement sensitivity, similar to that of Aura/OMI. Hence, OMPS NO_2 data have sufficient quality to continue and extend the existing Aura/OMI data records.

This achievement, facilitated by advances in retrieval algorithms, is unexpected since OMPS is designed primarily for measuring atmospheric total O_3 and does not have spectral coverage in the violet blue region (400–460 nm) typically used for DOAS NO_2 retrievals. Underlying this effort to improve satellite measurements of tropospheric composition is the long-term (> 15 years) data record expected from the global observations from OMPS on SNPP, JPSS-1, and JPSS-2, and the simultaneous and synergistic observations of NO_2 and SO_2, two criteria air pollutants identified by the U.S. Environmental Protection Agency, from the same instrument. The NO_2 and SO_2 products from OMPS will become more valuable as higher spatial resolution OMPS measurements are realized in the future JPSS-1 and JPSS-2 missions.

We plan to continue to improve the DVCF algorithm and STS scheme to achieve more accurate and sensitive retrievals of tropospheric NO_2. These improvements include the following: (1) a set of higher spatial resolution climatological tropospheric NO_2 profiles, identified in previous works [*Russell et al.*, 2011; *McLinden et al.*, 2013; *Lin et al.*, 2014] as one of the critical aspects for improving the DOAS NO_2 retrieval, (2) explicit treatment of aerosols and clouds in radiative transfer modeling of the radiance spectra, which has been demonstrated to improve tropospheric NO_2 retrieval [*Lin et al.*, 2014], (3) accounting for surface reflectance anisotropy [*Zhou et al.*, 2010; *Lin et al.*, 2014], (4) optimization of the STS scheme, and (5) extending DVCF algorithm for multilayer NO_2 retrieval by exploiting the broad range (> 100 nm) spectral responses [*Yang et al.*, 2010] to the variations in NO_2 vertical distributions. Validation and comparison with correlative measurements will be performed to identify errors and characterize uncertainties in OMPS NO_2 data.

Acknowledgments
We would like to thank both reviewers for their insightful comments, which helped us to considerably improve the manuscript. This work is supported by NASA. We acknowledge the use of OMPS Level 1B data produced by the SNPP Ozone Product Evaluation and Algorithm Test Element (PEATE), funded by NASA. OMPS data supporting figures in this paper are available at https://umd.box.com/DATA2014GL060136.

The Editor thanks two anonymous reviewers for their assistance in evaluating this paper.

References

Beirle, S., U. Platt, M. Wenig, and T. Wagner (2003), Weekly cycle of NO_2 by GOME measurements: A signature of anthropogenic sources, *Atmos. Chem. Phys.*, *3*, 2225–2232, doi:10.5194/acp-3-2225-2003.

Bey, I., D. J. Jacob, R. M. Yantosca, J. A. Logan, B. D. Field, A. M. Fiore, Q. Li, H. Y. Liu, L. J. Mickley, and M. G. Schultz (2001), Global modeling of tropospheric chemistry with assimilated meteorology: Model description and evaluation, *J. Geophys. Res.*, *106*(D19), 23,073–23,095, doi:10.1029/2001JD000807.

Boersma, K. F., et al. (2007), Near-real time retrieval of tropospheric NO_2 from OMI, *Atmos. Chem. Phys.*, *7*, 2103–2118, doi:10.5194/acp-7-2103-2007.

Bogumil, K., et al. (2003), Measurements of molecular absorption spectra with the SCIAMACHY pre-flight model: Instrument characterization and reference data for atmospheric remote-sensing in the 230–2380 nm region, *J. Photochem. Photobiol. A*, *157*, 167–184, doi:10.1016/S1010-6030(03)00062-5.

Bovensmann, H., J. P. Burrows, M. Buchwitz, J. Frerick, S. Noël, V. V. Rozanov, K. V. Chance, and A. P. H. Goede (1999), SCIAMACHY: Mission objectives and measurement modes, *J. Atmos. Sci.*, *56*, 127–150, doi:10.1175/1520-0469(1999)056<0127:SMOAMM>2.0.CO;2.

Brühl, C., and P. J. Crutzen (2000), NO_x-catalyzed ozone destruction and NO_x activation at midlatitudes to high latitudes as the main cause of the spring to fall ozone decline in the northern hemisphere, *J. Geophys. Res.*, *105*(D10), 12,163–12,168, doi:10.1029/2000JD900069.

Buchwitz, M., V. V. Rozanov, and J. P. Burrows (2000), A near-infrared optimized DOAS method for the fast global retrieval of atmospheric CH_4, CO, CO_2, H_2O, and N_2O total column amounts from SCIAMACHY Envisat-1 nadir radiances, *J. Geophys. Res.*, *105*(D12), 15,231–15,245, doi:10.1029/2000JD900191.

Bucsela, E., E. Celarier, M. Wenig, J. Gleason, P. Veefkind, K. F. Boersma, and E. Brinksma (2006), Algorithm for NO_2 vertical column retrieval from the Ozone Monitoring Instrument, *IEEE Trans. Geosci. Remote Sens.*, *44*, 1245–1258, doi:10.1109/TGRS.2005.863715.

Bucsela, E. J., N. A. Krotkov, E. A. Celarier, L. N. Lamsal, W. H. Swartz, P. K. Bhartia, K. F. Boersma, J. P. Veefkind, J. F. Gleason, and K. E. Pickering (2013), A new stratospheric and tropospheric NO_2 retrieval algorithm for nadir-viewing satellite instruments: Applications to OMI, *Atmos. Meas. Tech.*, *6*, 2607–2626, doi:10.5194/amt-6-2607-2013.

Burrows, J. P., A. Dehn, B. Deters, S. Himmelmann, A. Richter, S. Voigt, and J. Orphal (1998), Atmospheric remote-sensing reference data from GOME: Part 1. Temperature-dependent absorption cross-section of NO_2 in the 231–794 nm range, *J. Quant. Spectrosc. Radiat. Transfer*, *60*, 1025–1031, doi:10.1016/S0022-4073(97)00197-0.

Burrows, J. P., et al. (1999), The Global Ozone Monitoring Experiment (GOME): Mission concept and first scientific results, *J. Atmos. Sci.*, *56*, 151–175, doi:10.1175/1520-0469(1999)056<0151:TGOMEG>2.0.CO;2.

Cahalan, R. F., W. Ridgway, W. J. Wiscombe, S. Gollmer, and Harshvardhan (1994), Independent pixel and Monte Carlo estimates of stratocumulus albedo, *J. Atmos. Sci.*, *51*, 3776–3790, doi:10.1175/1520-0469(1994)051<3776:IPAMCE>2.0.CO;2.

Callies, J., E. Corpaccioli, M. Eisinger, A. Hahne, and A. Lefebvre (2000), GOME-2 MetOps second generation sensor for operational ozone monitoring, *ESA Bulletin*, *102*, 28–36.

Chance, K. (2006), Spectroscopic measurements of tropospheric composition from satellite measurements in the ultraviolet and visible: Steps toward continuous pollution monitoring from space, in *Remote Sensing of the Atmosphere for Environmental Security*, edited by A. Perrin, N. Ben Sari-Zizi, and J. Demaison, pp. 1–25, Springer, Dordrecht, Netherlands, doi:10.1007/978-1-4020-5090-9_1. ISBN 978-1-4020-5089-3.

Chance, K., and R. L. Kurucz (2010), An improved high-resolution solar reference spectrum for Earth's atmosphere measurements in the ultraviolet, visible, and near infrared, *J. Quant. Spectrosc. Radiat. Transfer*, *111*, 1289–1295, doi:10.1016/j.jqsrt.2010.01.036.

Chance, K., T. P. Kurosu, and C. E. Sioris (2005), Undersampling correction for array detector-based satellite spectrometers, *Appl. Opt.*, *44*(7), 1296–1304, doi:10.1364/AO.44.001296.

Choi, S., J. Joiner, Y. Choi, B. N. Duncan, and E. Bucsela (2014), Global free tropospheric NO_2 abundances derived using a cloud slicing technique applied to satellite observations from the Aura Ozone Monitoring Instrument (OMI), *Atmos. Chem. Phys. Discuss.*, *14*, 1559–1615, doi:10.5194/acpd-14-1559-2014.

Coldewey-Egbers, M., M. Weber, L. N. Lamsal, R. de Beek, M. Buchwitz, and J. P. Burrows (2005), Total ozone retrieval from GOME UV spectral data using the weighting function DOAS approach, *Atmos. Chem. Phys.*, *5*, 1015–1025, doi:10.5194/acp-5-1015-2005.

Dave, J. V. (1965), Multiple scattering in a non-homogeneous, Rayleigh atmosphere, *J. Atmos. Sci.*, *22*, 273–279, doi:10.1175/1520-0469(1965)022<0273:MSIANH>2.0.CO;2.

Hilboll, A., A. Richter, and J. P. Burrows (2013), Long-term changes of tropospheric NO_2 over megacities derived from multiple satellite instruments, *Atmos. Chem. Phys.*, *13*, 4145–4169, doi:10.5194/acp-13-4145-2013.

Lamsal, L. N., R. V. Martin, A. van Donkelaar, E. A. Celarier, E. J. Bucsela, K. F. Boersma, R. Dirksen, C. Luo, and Y. Wang (2010), Indirect validation of tropospheric nitrogen dioxide retrieved from the OMI satellite instrument: Insight into the seasonal variation of nitrogen oxides at northern midlatitudes, *J. Geophys. Res.*, *115*, D05302, doi:10.1029/2009JD013351.

Lee, C., A. Richter, M. Weber, and J. P. Burrows (2008), SO_2 Retrieval from SCIAMACHY using the Weighting Function DOAS (WFDOAS) technique: Comparison with Standard DOAS retrieval, *Atmos. Chem. Phys.*, *8*, 6137–6145, doi:10.5194/acp-8-6137-2008.

Levelt, P. F., G. H. J. van den Oord, M. R. Dobber, A. Mälkki, H. Visser, J. de Vries, P. Stammes, J. O. V. Lundell, and H. Saari (2006), The Ozone Monitoring Instrument, *IEEE Trans. Geosci. Remote Sens.*, *44*(5), 1093–1101, doi:10.1109/TGRS.2006.872333.

Leue, C., M. Wenig, T. Wagner, O. Klimm, U. Platt, and B. Jäne (2001), Quantitative analysis of NO_x emissions from Global Ozone Monitoring Experiment Satellite Image sequences, *J. Geophys. Res.*, *106*(D6), 5493–5505, doi:10.1029/2000JD900572.

Lin, J.-T., R. V. Martin, K. F. Boersma, M. Sneep, P. Stammes, R. Spurr, P. Wang, M. Van Roozendael, K. Clamer, and H. Irie (2014), Retrieving tropospheric nitrogen dioxide from the ozone monitoring instrument: Effects of aerosols, surface reflectance anisotropy, and vertical profile of nitrogen dioxide, *Atmos. Chem. Phys.*, *14*, 1441–1461, doi:10.5194/acp-14-1441-2014.

Martin, R. V., et al. (2002), An improved retrieval of tropospheric nitrogen dioxide from GOME, *J. Geophys. Res.*, *107*(D20), 4437, doi:10.1029/2001JD001027.

Martin, R. V., D. D. Parrish, T. B. Ryerson, D. K. Nicks Jr., K. Chance, T. P. Kurosu, D. J. Jacob, E. D. Sturges, A. Fried, and B. P. Wert (2004), Evaluation of GOME satellite measurements of tropospheric NO_2 and HCHO using regional data from aircraft campaigns in the southeastern United States, *J. Geophys. Res.*, *109*, D24307, doi:10.1029/2004JD004869.

McLinden, C. A., V. Fioletov, K. F. Boersma, S. K. Kharol, N. Krotkov, L. Lamsal, P. A. Makar, R. V. Martin, J. P. Veefkind, and K. Yang (2013), Improved satellite retrievals of NO_2 and SO_2 over the Canadian oil sands and comparisons with surface measurements, *Atmos. Chem. Phys. Discuss.*, *13*, 21,609–21,664, doi:10.5194/acpd-13-21609-2013.

Munro, R., M. Eisinger, C. Anderson, J. Callies, E. Corpaccioli, R. Lang, A. Lefebvre, Y. Livschitz, and A. Perez Albinana (2006), GOME-2 on MetOp, paper presented at EUMETSAT Meteorological Satellite Conference, Helsinki, Finland, 12–16 June.

Palmer, P. I., D. J. Jacob, K. Chance, R. V. Martin, R. J. D. Spurr, T. P. Kurosu, I. Bey, R. Yantosca, A. Fiore, and Q. Li (2001), Air mass factor formulation for spectroscopic measurements from satellites: Application to formaldehyde retrievals from the Global Ozone Monitoring Experiment, *J. Geophys. Res.*, *106*(D13), 14,539–14,550, doi:10.1029/2000JD900772.

Platt, U. (1994), Differential optical absorption spectroscopy (DOAS), *Chem. Anal. Ser.*, *127*, 27–83.

Richter, A., and J. P. Burrows (2002), Retrieval of tropospheric NO_2 from GOME measurements, *Adv. Space Res.*, *29*, 1673–1683.

Richter, A., J. P. Burrows, H. Nüß, C. Granier, and U. Niemeier (2005), Increase in tropospheric nitrogen dioxide over China observed from space, *Nature*, *437*, 129–132, doi:10.1038/nature04092.

Richter, A., M. Begoin, A. Hilboll, and J. P. Burrows (2011), An improved NO_2 retrieval for the GOME-2 satellite instrument, *Atmos. Meas. Tech.*, *4*, 1147–1159, doi:10.5194/amt-4-1147-2011.

Russell, A. R., A. E. Perring, L. C. Valin, E. J. Bucsela, E. C. Browne, P. J. Wooldridge, and R. C. Cohen (2011), A high spatial resolution retrieval of NO_2 column densities from OMI: Method and evaluation, *Atmos. Chem. Phys.*, *11*, 8543–8554, doi:10.5194/acp-11-8543-2011.

Seftor, C. J., G. Jaross, M. Kowitt, M. Haken, J. Li, and L. E. Flynn (2014), Postlaunch performance of the Suomi National Polar-orbiting Partnership Ozone Mapping and Profiler Suite (OMPS) nadir sensors, *J. Geophys. Res. Atmos.*, *119*, 4413–4428, doi:10.1002/2013JD020472.

Seinfeld, J. H., and S. N. Pandis (2006), *Atmospheric Chemistry and Physics: From Air Pollution to Climate Change*, 2nd ed., John Wiley, New York, ISBN 978-0-471-72018-8.

Spurr, R. J. D., J. de Haan, R. van Oss, and A. P. Vasilkov (2008), Discrete ordinate radiative transfer in a stratified medium with first order rotational Raman scattering, *J. Quant. Spectrosc. Radiat. Transfer*, *109*(3), 404–425.

Vandaele, A. C., C. Hermans, P. C. Simon, M. Carleer, R. Colin, S. Fally, M. F. Merienne, A. Jenouvrier, and B. Coquart (1998), Measurements of the NO_2 absorption cross-section from 42000 cm^1 to 10000 cm^1 (238–1000 nm) at 220 K and 294 K, *J. Quant. Spectrosc. Radiat. Transfer*, *59*, 171–184, doi:10.1016/S0022-4073(97)00168-4.

Velders, G. J. M., C. Granier, R. W. Portmann, K. Pfeilsticker, M. Wenig, T. Wagner, U. Platt, A. Richter, and J. P. Burrows (2001), Global tropospheric NO_2 column distributions: Comparing three-dimensional model calculations with GOME measurements, *J. Geophys. Res.*, *106*(D12), 12,643–12,660, doi:10.1029/2000JD900762.

Yang, K., N. A. Krotkov, A. J. Krueger, S. A. Carn, P. K. Bhartia, and P. F. Levelt (2007), Retrieval of large volcanic SO_2 columns from the Aura Ozone Monitoring Instrument: Comparison and limitations, *J. Geophys. Res.*, *112*, D24S43, doi:10.1029/2007JD008825.

Yang, K., N. A. Krotkov, A. J. Krueger, S. A. Carn, P. K. Bhartia, and P. F. Levelt (2009a), Improving retrieval of volcanic sulfur dioxide from BUV satellite observations, *Geophys. Res. Lett.*, *36*, L03102, doi:10.1029/2008GL036036.

Yang, K., X. Liu, N. A. Krotkov, A. J. Krueger, and S. A. Carn (2009b), Estimating the altitude of volcanic sulfur dioxide plumes from spaceborne hyperspectral UV measurements, *Geophys. Res. Lett.*, *36*, L10803, doi:10.1029/2009GL038025.

Yang, K., X. Liu, P. K. Bhartia, N. A. Krotkov, S. A. Carn, E. J. Hughes, A. J. Krueger, R. J. D. Spurr, and S. G. Trahan (2010), Direct retrieval of sulfur dioxide amount and altitude from spaceborne hyperspectral UV measurements: Theory and application, *J. Geophys. Res.*, *115*, D00L09, doi:10.1029/2010JD013982.

Yang, K., R. R. Dickerson, S. A. Carn, C. Ge, and J. Wang (2013), First observations of SO_2 from the satellite Suomi NPP OMPS: Widespread air pollution events over China, *Geophys. Res. Lett.*, *40*, 4957–4962, doi:10.1002/grl.50952.

Zhou, Y., D. Brunner, R. J. D. Spurr, K. F. Boersma, M. Sneep, C. Popp, and B. Buchmann (2010), Accounting for surface reflectance anisotropy in satellite retrievals of tropospheric NO_2, *Atmos. Meas. Tech.*, *3*, 1185–1203, doi:10.5194/amt-3-1185-2010.